View metadata, citation and similar papers at core.ac.uk

brought to you by CORE

provided by NASA Technical Reports Server

X-646-71-473

PREPRINT

NASA TM X- 65786

THE GEOMETRIC FACTOR OF A CYLINDRICAL PLATE ELECTROSTATIC ANALYZER

A. D. JOHNSTONE

FEB 1972 RECEIVED NASA STI FACILITY INPUT BRANCH

NOVEMBER 1971

GSFC — GODDARD SPACE FLIGHT CENTER — MARYLAND

(NASA-TM-X-65786) THE GEOMETRIC FACTOR OF A CYLINDRICAL PLATE ELECTROSTATIC ANALYZER A.D. Johnstone (NASA) Nov. 1971 55 p CSCL 14B

N72-15423

Unclas 13351

G3/14

FACILITY FORM TMX 65786 (NASA CR OR TMX OR AD NUMBER)

(CODE) 14 (CATEGORY)

THE GEOMETRIC FACTOR OF A CYLINDRICAL PLATE ELECTROSTATIC ANALYZER

A. D. Johnstone

NOVEMBER 1971

ABSTRACT

A method for calculating the geometric factor of cylindrical-plate electrostatic energy analyzers with various detector geometries is described. The effects of the fringe-field are estimated. For a special simple case an exact geometric factor is calculated enabling an estimate of the inaccuracies of the approximations used in other cases. The results of some calculations are presented and a simple approximate expression for the geometric factor is deduced.

1. INTRODUCTION

One of the most important reservoirs of energy in the Earth's magnetosphere is the population of trapped particles, predominantly protons and electrons with energies from 10 eV to 100 keV. The solar wind which controls the formation of the magnetosphere is also composed of particles in this energy range. The measurement of low fluxes of such particles from space vehicles required the development of new detection techniques. Channel electron multipliers[1], used for this purpose now for several years with great success, provide no information about the energy of the particles. Hence energy analyzers, which allow only those particles within a prescribed energy range to reach the detector, must also be used. The most popular analyzers have been electrostatic analyzers with either two concentric spherical[2-4], or two coaxial cylindrical plates[6-9]. Other electrostatic analyzers[10-11], and magnetic analyzers[12], have been used successfully.

Curved plate analyzers have been used in the laboratory for many years and many papers have published[13-15], and continue to be published analyzing their performance. In the laboratory the particle source is usually discrete and the analyzer's most important properties are its energy resolution and focusing action. In space use the source is diffuse, extended and has a wide range of energies. Its important properties are then its energy bandwidth and geometric factor. A different analysis is required. In this paper these properties of cylindrical plate analyzers are calculated theoretically.

Other authors [16];[17] have described methods of calculating geometric factors but none have the degree of completeness of that described here.

Using this method it is possible to allow for the precise shape of the detector and if necessary for variations in efficiency across its surface. This is an important advantage of the method when channel electron multipliers are used as the detector. The effect of the fringing field at the ends of the analyzer plates is estimated and the validity of approximations used is checked.

Theodoridis and Paolini[16] in their calculation adapted a method originally applied to spherical plate analyzers but it is doubtful whether the trajectory equation they use is valid for a reason that is discussed below. Reidler's[17] calculation is based on a trajectory equation similar to the one used here but like Theodoridis and Paolini[16] he cannot allow for the shape of the detector or the fringing field. Other workers of the authors acquaintance have made unpublished calculations based on tracing a trajectory numerically through the analyzer. The method requires extensive and time-consuming computation compared with the much simpler method described here.

The method has been applied to a number of different practical analyzers and from the results an approximate expression for the geometric factor and energy bandwidth of any analyzer within a prescribed range of the central angle is obtained. This enables a cylindrical analyzer with any desired characteristics to be designed rapidly.

The following is a list of the symbols used most frequently. Others are defined where used. The analyzer geometry is shown in Figures 1 and 12.

r	radial coordinate
$\bar{r}$	radius of surface at zero potential
$\rho = r/\bar{r}$	dimensionless radial coordinate
M	radial position where $K(\rho) = 1$ (eq. 3.4)
θ	angular coordinate measured from entrance to analyzer plates
θ_p	sector angle of analyzer plates
α	angle between tangent and trajectory
T_p	kinetic energy of circular orbit which is used as the unit of energy for the following quantities.
E	total energy of the particle
H	particle energy in the plane perpendicular to the cylindrical axis
$R(\rho)$	kinetic energy of radial motion
$K(\rho)$	total kinetic energy
T	kinetic energy associated with azimuthal motion at $\rho = 1$
e,m	charge and mass of the particle
L	angular momentum of the particle
Δ	analyzer plate spacing/mean plate diameter
x,m	defined by equations 4.10
$GF(E)$	energy dependent geometric factor
$[GF]$	energy-integrated geometric factor at unit energy
B	fractional energy bandwidth
Y,y,ℓ, χ	are various dimensions of the analyzer/detector defined in Figures 1 and 12

subscripts

$\perp, \parallel$	refer to motion perpendicular and parallel to the cylindrical axis

o,i refer to the outer and inner analyzer plates

1,2 refer to quantities calculated for outer and inner orbital radial limits.

2. GENERAL CONSIDERATIONS

The directional intensity of particles in a distribution is $I(\vec{x}, \hat{v}, E)$ usually expressed in units of $cm^{-2}ster^{-1}eV^{-1}sec^{-1}$, where $\vec{x}$ is a position vector and $\hat{v}$ is a unit vector in the direction of particle motion. The counting rate CR, in units sec^{-1}, of an analyzer/detector measuring particles in this distribution is

$$CR = \int I \cos \alpha \; g \; (\vec{x}, \hat{v}, E) \; dS d\Omega dE$$

where α is the angle of incidence of the particle on the element of surface dS. The function $g(\vec{x}, \hat{v}, E)$ has the value unity for values of $\vec{x}$, $\hat{v}$, E corresponding to trajectories which strike the detector and zero otherwise. It is used only as a device to express simply the limits of integration over solid angle and energy. The surface integral is taken over any surface which is crossed once and only once by each trajectory reaching the detector. Usually this is the entrance aperture of the analyzer.

The energy-dependent geometric factor is defined by

$$GF(E) = \int g \cos \alpha \; dS d\Omega \qquad 2.1$$

in units of cm^2ster and the energy-integrated geometric factor by

$$[GF] = \int GF(E) \; dE \qquad 2.2$$

where the units of [GF] are cm^2ster eV. Both quantities are functions of the geometry of the analyzer/detector only. Since each particle striking the detector produces the same response the variation of I within the range of acceptance of the detector cannot be measured. Hence the observed intensity I_{obs}, given by

$$I_{obs} = CR/[GF]$$

is an approximation to the real intensity. If the energy-bandwidth is large a better result may be obtained by integrating an assumed spectral shape I'(E) over the energy-dependent geometric factor to find the magnitude of the intensity A.

$$A = CR/\int I'(E)\ GF(E)\ dE$$

Alternatively, when an energy spectrum is measured with several analyzers an iterative procedure can be followed by putting $I'(E) = I_{obs}(E)$.

Both GF(E) and [GF] are calculated here. From GF(E) the energy-bandwidth B, defined to be the full-width at half maximum, can be found.

As already mentioned it is normal in calculating geometric factors to take the surface integral over the entrance aperture of the analyzer. Until crossing this surface the particles follow a trajectory which is independent of the presence of the analyzer. Theodoridis and Paolini[5] and Reidler[6] tacitly assume the entrance to the plates to be equivalent except for a change in the energy of particles entering the plates away from the zero potential surface. This is not completely accurate. In

Figure 2 the trajectories of a group of particles through a two dimensional analyzer are shown in a general way in configuration and velocity space. At point P, in free space the particles occupy a contiguous volume element in the four-dimensional phase space. According to Liouville's theorem the volume will remain contiguous and the same size at all points along the group of trajectories. At point P the volume is that filled by all the particles crossing the line dx_1, in angular range $d\alpha_1$, velocity range dv_1, in time dt, where dx_1 is perpendicular to the group of trajectories.

$$dx_1 \, d\alpha_1 \, v_1^2 \, dv_1 \, dt = dx_2 \, d\alpha_2 \, \underline{v}_2^2 \, dv_2 \, dt \qquad 2.3$$

where subscript 2 indicates point Q. An electric potential difference ϕ_{PQ} exists between P and Q so that

$$\tfrac{1}{2} m v_1^2 = \tfrac{1}{2} m v_2^2 + e\phi_{PQ}$$

Differentiating,

$$v_1 \, dv_1 = v_2 \, dv_2 \qquad 2.4$$

From 2.3, 2.4

$$dx_1 \, d\alpha_1 = N \, dx_2 \, d\alpha_2 \qquad 2.5$$

where $N = v_2 / v_1$.

By using equation 2.5 the surface integral in equation 2.1 can be taken over any suitable surface. The most convenient is the exit plane from the analyzer plates, immediately in front of the sensitive surface of the detector. It is then possible to allow for the particular shape

of the detector although it is harder to allow for the shape of the entrance aperture and any collimating structure. Since the collimator is outside the fringing field, in which the trajectories are deflected by an unknown amount, it cannot be allowed for accurately anyway. In these calculations it is assumed that there is no obstruction to particles near the entrance and that the only restrictions on the particles are the curved plates and the sensitive surface of the detector. Analyzers which meet this requirement have been used by the author.

The calculation for the three dimensional analyzer is simplified by resolving the motion into two perpendicular surfaces. In each a geometric factor with the dimensions of length times angle is calculated. The total geometric factor is then approximately the product of the two partial factors. This approximation is good for the small solid angles normally found in electrostatic analyzers. The two surfaces chosen are a plane perpendicular to the axis of the cylinder (the Z axis) and the cylindrical surface ($r = \bar{r}$) at zero potential between the deflecting plates of the analyzer. Motion on the cylindrical surface is not affected by the radial electric field between the plates. The geometric factor is calculated in each surface by finding the extreme angles of incidence at the detector surface of trajectories which pass through the analyzer. Then from 2.1

$$\delta(GF) = N\delta s \int_{-\alpha_2}^{\alpha_1} \cos\alpha \, d\alpha$$

where δs is a line element of the detector surface.

$$\delta(GF) = N\delta s \, (\sin\alpha_1 + \sin\alpha_2) \qquad 2.6$$

3. MOTION PERPENDICULAR TO THE CYLINDRICAL AXIS

The Hamiltonian H' for particle motion between the analyzer plates in the Z=0 plane is

$$H' = p_r^2/2m + p_\theta^2/2mr^2 + eQ\log(r/\bar{r})$$

where $$Q = (V_o - V_i) \log (r_o/r_i)$$

and the $r=\bar{r}$ surface is at zero potential. It is assumed throughout that the voltages on the plates are symmetrical, i.e., $V_o = -V_i$ so that

$$\bar{r}^2 = r_o r_i$$

The extension to analyzers with nonsymmetrical voltages is discussed in Section 8. Since $(r_o - r_i) \ll \bar{r}$ for most practical analyzers $\bar{r} \approx (r_o + r_i)/2$.

θ is a cyclic coordinate in H' so that p_θ is conserved and may be put equal to L. H' is also conserved and is equal to the total energy of the particle, excluding motion perpendicular to the plane.

If the electric field was infinite in radial extent, and not limited by the analyzer plates, the motion of all the particles would remain bounded because as $r \to o$, $L^2/mr^2 \to \infty$ and as $r \to \infty$, $eQ\log(r/\bar{r}) \to \infty$.[18] The radial limits of an orbit, r_K, are given by $p_r = 0$

$$H' = L^2/2mr_K^2 + eQ\log(r_K/\bar{r}) \qquad 3.1$$

The particle's radial motion is oscillatory between the two solutions of equation 3.1.

If $H' = L^2/2m\bar{r}^2 = eQ/2$ it is readily shown that the particle is in a circular orbit with kinetic energy T_p

$$T_p = L^2/2m\bar{r}^2 = eQ/2$$

It is a property of the cylindrical analyzer that T_p is independent of the radius of the orbit. The Hamiltonian may be written in dimensionless form as an energy equation

$$H = R + T/\rho^2 + 2 \log \rho \qquad 3.2$$

where

$$R = \tfrac{1}{2} m\dot{r}^2/T_p$$

$$T = L^2/2m\bar{r}^2T_p$$

$$H = H'/T_p$$

$$\rho = r/\bar{r}$$

The parameters H and T are constants of the motion between the analyzer plates. H is the total energy of the particle and is its kinetic energy before it enters the analyzer for motion in the Z=0 plane, and T is a function of the angular momentum L. Equation 3.1 becomes

$$H = T/\rho_K^2 + 2\log\rho_K \qquad 3.3$$

When H = 1 the set of solutions of Equation 3.3 can be denoted formally by

$$\rho_K = \rho_{10}(T) \qquad \text{outer radial limit}$$

$$= \rho_{20}(T) \qquad \text{inner radial limit}$$

As $T \rightarrow 1$, $\rho_{10} \rightarrow \rho_{20}$. If $H \neq 1$ the solutions can still be written in terms of ρ_{10} and ρ_{20} by putting

$$H = 1 + 2 \log M$$
$$T = T'M^2 \qquad 3.4$$

Then from (3.3)

$$1 = T' \frac{M^2}{\rho_K^2} + 2 \log \left(\frac{\rho_K}{M}\right)$$

for which the solutions are

$$\rho_1 = M\rho_{10}(T/M^2)$$
$$\rho_2 = M\rho_{20}(T/M^2) \qquad 3.5$$

M is the radius where the kinetic energy of the particle is T_p, the energy required for a circular orbit. All orbits are geometrically similar with the magnitudes scaled according to Equations 3.5. Some values of $\rho_{10}(T)$ and $\rho_{20}(T)$ have been obtained by a numerical solution of (3.3) and are listed in Table 1. The two right-hand columns of the table show that

$$\rho_{10} \approx 1 + A(T)$$
$$\rho_{20} \approx 1 - A(T)$$

where A(T) is the amplitude of the radial oscillation
As a quantitative check on the validity of this approximation the quantity ν has been plotted in Figure 3.

$$\nu = \frac{2 - (\rho_{10} + \rho_{20})}{\rho_{10} - \rho_{20}}$$

It is the difference between the arithmetic mean of the trajectory limits and the circular orbit radius expressed as a fraction of the amplitude of the oscillation. In most practical analyzers the amplitude

of the oscillation of allowed trajectories is less than the range covered in Figure 3 in which ν has a maximum value of 0.025. Using this approximation and recalling that the motion is oscillatory between these limits a first approximation to the trajectory equation can be written

$$\rho = M\,(1 + A \cos\,(K\theta + \eta)) \qquad 3.6$$

If A is a function of (T/M^2) the trajectory shows the correct scaling properties as in Equations 3.5. Hughes and Rojansky[13] have shown that the cylindrical analyzer focuses the particles at $\theta = \pi/\sqrt{2}$ (127° 17'). If $K = \sqrt{2}$ the trajectory of Equation 3.6 has the same property. Consider, following Hughes and Rojansky, particles entering the analyzer at $\theta = 0$ with $\rho = 1$, $H = 1$ at an angle to the tangent (i.e., non-zero A) then from (3.6)

$$A \cos \eta = 0$$

$$\therefore \quad \eta = (2n + 1)\,\pi/2$$

At $\quad \theta = \pi/\sqrt{2},\ (127^\circ\ 17')$

$$\rho = 1 + A \cos\,[(2n + 3)\,\tfrac{\pi}{2}] = 1$$

for all values of A, where n is an integer. The sinusoidal form for the trajectory equation, obtained here almost empirically, was derived originally by Hughes and Rojansky, with the difference that their radial variable was $u \equiv \rho^{-1}$, by an approximate solution of the differential equation of the trajectory. Reidler[17] achieved the same result with an approximate integration of the equations of motion. Theodoridis and Paolini[16] approximate

the trajectory with a circle. However, such trajectories focus at $\theta = 180^{o}$. It seems unlikely that the approximation could give accurate geometric factors, particularly its variation with θ_p, if it fails to reproduce the gross properties of the analyzer. The accuracy of the sinusoidal approximation is estimated in Section (5).

4. CALCULATION OF GF⊥

Figures 4 through 6 illustrate, for different cases, the allowed trajectories with the greatest angles of incidence (α_1, $-\alpha_2$) at the detector surface. These trajectories are referred to as limiting trajectories. All intermediate angles of incidence are allowed. The criteria used to determine the limiting trajectory vary with the angle θ_p of the analyzer. Four cases are considered below.

1. When $\theta_p > \sqrt{2\pi}$ each trajectory must have passed two radial turning points between the plates. Only trajectories with $\rho_1 < \rho_o$ and $\rho_2 > \rho_i$ are able to reach the detector. Figure 4 shows that when $M > 1$ the

limiting trajectory for both α_1 and α_2 grazes the outer plate and that $\alpha_1=\alpha_2$. Similarly when $M < 1$ the limiting trajectory grazes the inner plate. The angle of incidence of the limiting trajectory is given by

$$\sin \alpha_K = \left(\frac{R(\rho)}{K(\rho)} \right)^{\frac{1}{2}}$$

where $K(\rho)$ is the particle's kinetic energy at ρ. ρ is the radial position of a detector element. $N = \sqrt{K/H}$, therefore from 2.6

$$\delta(GF_\perp) = 2\ \bar{r}\ d\rho \left(\frac{R(\rho)}{H} \right)^{\frac{1}{2}} \qquad 4.1$$

From 3.2 and 3.3 for trajectories which graze the outer plate

$$R_1(\rho) = (H/\rho^2)(\rho^2-\rho_o^2) + (2/\rho^2)(\rho_o^2 \log \rho_o - \rho^2 \log \rho) \qquad 4.2$$

When the trajectory grazes the inner plate subscript o is replaced by i to give $R_2(\rho)$. No approximation is involved in this equation for $R(\rho)$.

2. When $\theta_p = \pi/\sqrt{2}$ each trajectory passes one and only one radial turning point between the plates. From Figure 5 it is clear that the limiting angles of incidence are given by

$$N \sin \alpha_1 = \left(\frac{R_1(\rho)}{H} \right)^{\frac{1}{2}} \qquad 4.3a$$

$$N \sin \alpha_2 = \left(\frac{R_2(\rho)}{H} \right)^{\frac{1}{2}} \qquad 4.3b$$

Using Equations 4.3 in 2.6 enables $GF_\perp$ to be calculated without approximation when $\theta_p = \pi/\sqrt{2}$.

3. When $\pi/2\sqrt{2} < \theta_p < \pi/\sqrt{2}$ some trajectories pass through the analyzer without reaching a turning point. Referring to Figure 6, one limit is always set by a trajectory which grazes a plate at its turning point. When $\rho > M$ it grazes the outer plate and α_1 is given by (4.3a) and when $\rho < M$ it grazes the inner plate and α_2 is given by (4.3b). In some circumstances, discussed later, the other limit is set by a trajectory which grazes a plate at the entrance and never passes a turning point between the plates. An example is shown in Figure 6. The approximate trajectory equation must be used to find the angle of incidence.

4. For the fourth case, analyzers with $\theta_p < \pi/2\sqrt{2}$, both limits may be set by trajectories grazing a plate at the entrance. One limit, but never both simultaneously, can be set by a trajectory reaching a turning point.

In this paper the geometric factor of analyzers with $\pi/2\sqrt{2} \leq \theta_p \leq \pi/\sqrt{2}$, the third case, is calculated. The method may be extended equally well to any of the other cases.

Using the approximate trajectory Equation (3.6) the angle of incidence is

$$\alpha = \tan^{-1}\left(\frac{\sqrt{2}\,MA \sin(\sqrt{2}\,\theta_p + \eta)}{\rho}\right) \qquad 4.4$$

When the limiting trajectories graze the plate at a turning point,

$$\rho_o = M(1+A) \quad \text{or} \quad \rho_i = M(1-A) \qquad 4.5$$

Approximating N sin $\alpha \approx \tan \alpha$ (an approximation whose accuracy is considered later) from 4.4, 4.5

$$N \sin \alpha_1 = \frac{\sqrt{2}}{\rho\sqrt{H}} \left((\rho_o - M)^2 - (\rho - M)^2\right)^{\frac{1}{2}} \qquad 4.6a$$

$$N \sin \alpha_2 = \frac{\sqrt{2}}{\rho\sqrt{H}} \left((\rho_i - M)^2 - (\rho - M)^2\right)^{\frac{1}{2}} \qquad 4.6b$$

When the limiting trajectory grazes the outer plate at the entrance, $\theta = 0$ and

$$\rho_o = M(1+A \cos \eta) \qquad 4.7$$

at $\theta = \theta_p$

$$\rho = M(1+A \cos (\sqrt{2}\, \theta_p + \eta)) \qquad 4.8$$

From 4.4, 4.7, 4.8

$$N \sin \alpha_1 = \frac{\sqrt{2}}{\rho\sqrt{H}} \left(\frac{(\rho_o - M) - (\rho - M) \cos (\sqrt{2}\, \theta_p)}{\sin (\sqrt{2}\, \theta_p)} \right) \qquad 4.9a$$

Similarly when the trajectory grazes the inner plate

$$N \sin \alpha_2 = \frac{\sqrt{2}}{\rho\sqrt{H}} \left(\frac{(\rho_i - M) - (\rho - M) \cos \sqrt{2}\, \theta_p)}{\sin \sqrt{2}\, \theta_p} \right) \qquad 4.9b$$

Equations 4.6, 4.9 may be simplified by putting $(\rho_o - 1) \approx (1 - \rho_i) = \Delta$ and

$$(M-1)/\Delta = m$$

$$(\rho-1)/\Delta = x$$

$$\sqrt{2}\, \Delta/\rho\sqrt{H} = C$$

then

$$N \sin \alpha_1 = C\,((1-m)^2 - (x-m)^2)^{\frac{1}{2}} \qquad 4.10a$$

$$\text{or} \qquad = C\left(\frac{(1-m) - (x-m)\cos\sqrt{2}\,\theta_p}{\sin\sqrt{2}\,\theta_p}\right) \qquad 4.10b$$

$$N \sin \alpha_2 = C((1+m)^2 - (x-m)^2)^{\frac{1}{2}} \qquad 4.11a$$

$$\text{or} \qquad = C\left(\frac{-(1+m) - (x-m)\cos\sqrt{2}\,\theta_p}{\sin\sqrt{2}\,\theta_p}\right) \qquad 4.11b$$

The next problem is to find out when the limiting trajectory grazes the plate at its turning point and when it grazes the entrance. Figure 7 illustrates a trajectory which grazes the outside plate both at its turning point and at the entrance. For this trajectory both expressions 4.10a,b give the same value for N sin α_1. Then

$$x-m = (1-m)\cos\sqrt{2}\,\theta_p \qquad 4.12a$$

This curve in x,m space is the boundary between the regions in which 4.10a,b are used. If $x-m > (1-m)\cos\sqrt{2}\,\theta_o$ 4.10a gives the limiting trajectory. Similarly the boundary between the regions of validity for 4.11a,b is

$$x-m = -(1+m)\cos\sqrt{2}\,\theta_p \qquad 4.12b$$

If $x-m > -(1+m)\cos\sqrt{2}\,\theta_p$ 4.11b is the correct expression.

As m increases beyond the value given by 4.12a the value of N sin α_1 given by 4.10b becomes negative. An example of such a trajectory is shown in Figure 8. Eventually

$$N \sin \alpha_1 + N \sin \alpha_2 = 0$$

when from 4.10b, 4.11a

$$x-m = (1-m)\cos\sqrt{2}\,\theta_p - 2\sqrt{m}\sin\sqrt{2}\,\theta_p \qquad 4.13a$$

This value of m marks the upper energy cut-off of the analyzer for the particular value of x. Similarly at the lower energy cut-off, from 4.10a, 4.11b

$$x-m = -(1+m)\cos\sqrt{2}\,\theta_p + 2\sqrt{-m}\sin\sqrt{2}\,\theta_p \qquad 4.13b$$

Figure 9 shows curves 4.12, 4.13 in x,m space for three values of θ_p. Also included are the lines $x = \pm 1$ which represent the surface of the plates. Table 2 lists the correct expressions for α_1, α_2 in each region of the diagram. When $\theta_p = \pi/\sqrt{2}$ curves 4.12a, 4.12b are identical with 4.13a, 4.13b respectively and there is only the region B in the diagram. This is case 2 discussed above. When $\theta_p = \pi/2\sqrt{2}$ curves 4.12a and 4.12b are identical and region B disappears. At smaller values of θ_p, 4.12a and 4.12b change positions.

5. THE ACCURACY OF THE APPROXIMATE TRAJECTORY EQUATION

The trajectory equation is required in the analysis to find those limiting trajectories which graze a plate at the entrance. For consistency it has been used throughout to find the angles of incidence of all the trajectories. The path difference between the actual and approximate trajectories cannot be calculated easily but the angle between the trajectory and the tangent to the cylindrical surface can be calculated exactly from 4.3 and from the approximate equation. When H=1, from 4.2.

$$\sin^2\alpha = \frac{R(\rho)}{K(\rho)} = 1 - \frac{\rho_o^2(1-2\log\rho_o)}{\rho^2(1-2\log\rho)}$$

and from 4.6 $\tan \alpha = \sqrt{2}\ \Delta\ (1-x^2)^{\frac{1}{2}}/\rho$

If the two values of $\alpha(\rho)$ were identical the trajectories would have to be identical. The value of $\alpha(\rho)$ given by each expression is plotted in Figure 10 for a trajectory with a relatively large amplitude oscillation $(\rho_1 - \rho_2) \approx 0.2$. The greatest fractional difference except near the inner limit, is of the order of 0.1. In Table 3, N sin α is calculated for the same trajectory from Equations 4.3 and compared with tan α obtained from Equation 4.6. It was found that tan α gave closer agreement for the angles of incidence than any other simple function. From the scaling properties of the real and approximate solutions all trajectories with the same relative amplitude have the same relative difference between real and approximate trajectories. Further calculations show that trajectories with smaller oscillations agree more closely. The trajectory examined here is an extreme case for most practical analyzers.

For one special case the geometric factor can be calculated without using the trajectory equation. All the limiting trajectories of an analyzer with $\theta_o = \pi/\sqrt{2}$ graze the plates at turning points. Then Equations 4.2, 4.3 can be used throughout. Table 4 lists the energy-integrated geometric factor $[GF_\perp]$ for four such analyzers calculated both ways. Even for $\Delta = 0.1$ the difference is less than 1%. When the energy-dependent geometric factor is examined slightly greater differences are found. The

quantity $\epsilon(H)$ is defined as

$$\epsilon(H) = 2\left(\frac{GFE_{\perp}(H) - GFA_{\perp}(H)}{GFE_{\perp}(H) + GFA_{\perp}(H)}\right)$$

$GFE_{\perp}$ is the exact and $GFA_{\perp}$ the approximate value of $GF_{\perp}(H)$. $\epsilon(H)$ is shown in Figure 11 for the analyzers of Table 4. Except for energy range (marked in the diagram) all the curves are identical. They are very nearly linear and anti-symmetric, hence the small effect on $[GF_{\perp}]$.

6. MOTION PARALLEL TO THE AXIS

Since there is no electric field parallel to the Z-axis the particle velocity in the Z direction remains constant. If the plate spacing is small the angular velocity about the axis is nearly constant so that the motion projected on the $r=\bar{r}$ surface (Figure 12) can be approximated as that of a particle with a constant pitch angle $(\pi/2 - \chi)$. The length of a detector element width $\bar{r}\, d\rho$ parallel to the axis is $y(\rho)$. The distance between the entrance aperture and the detector around the curve is $\ell(\rho)$. Its variation with ρ is ignored here because the separation of the plates is small. If the length of the entrance aperture parallel to the Z-axis is Y then the amount of the strip y accessible to particles with pitch angle $(\pi/2 - \chi)$ is $y(\chi)$ where

$$y(\chi) = y \text{ if } |\tan\chi| < \left(\frac{Y-y}{\ell}\right)$$

$$y(\chi) = (Y+y - \ell\tan\chi) \text{ if } \frac{Y-y}{\ell} < |\tan\chi| < \frac{Y+y}{\ell}$$

and $$y(\chi) = 0 \text{ if } |\tan\chi| > \frac{Y+y}{\ell} \qquad 6.1$$

If y is symmetrically placed with respect to the entrance aperture, as is assumed here then

$$\delta(GF//) = 2y\ (\chi,\rho)\ \cos\ \chi\ d\chi \qquad 6.2$$

If y is not symmetrical the calculation is more complicated but not changed in principle.

If the detector efficiency is less than unity, and perhaps variable across its surface, it can be allowed for by an extra factor in Equation 6.2.

7. TOTAL GEOMETRIC FACTOR

An element of the total geometric factor is

$$\delta(GF) = \delta(GF_{\perp})\ \delta(GF/\!/)$$

Writing equation 4.10 and 4.11 in the form

$$N \sin \alpha_K = \frac{\sqrt{2}\Delta}{\rho \sqrt{H}}\ G_K\ (\chi,m)$$

then

$$\delta(GF) = 2\sqrt{2}\ \Delta^2\ \bar{r} \sum_{K=1,2} \frac{G_K(\chi,m)}{\rho\sqrt{H}}\ y(x,\chi) \cos\chi\ d\chi dx \qquad 7.1$$

The total kinetic energy of the particle outside the analyzer is E and its component associated with motion in the plane perpendicular to the axis is H,

$$H = E \cos^2\chi$$

The geometric factor at constant E is required so that 7.1 must be integrated with E constant. m is a function of H and thus χ in the integration. In general 7.1 must be integrated numerically although in some simple cases part of the integration can be carried out directly. A computer program has been written to perform the integration. Some results are given in the next section.

A program listing in FORTRAN is available.

8. RESULTS

1. The energy bandwidth, defined as the full-width at half-maximum of GF(E) (see Figure 15) in units of T_p the kinetic energy of a circular orbit, is proportional to Δ. This is obvious from the form of Equations 4.10, 4.11. The variables m and H are functions of energy and determine the bandwidth of the integrated expressions. The dependence on H is weak and m is the dominant variable. Since $m \approx (\sqrt{H}-1)/\Delta$ the energy bandwidth is proportional to Δ.

2. The bandwidth B is a strong function of θ_p as is shown qualitatively by Figure 9. The quantity B/Δ has been plotted in Figure 14 for the analyzers listed in Table 5. The straight line fitted to the points on a logarithmic scale shows that in the range $60^o < \theta_p < 125^o$ the bandwidth may be approximated by

$$B/\Delta = 2.36 \times 10^5 \, \theta_p^{-2.43}$$

3. The bandwidth is only weakly dependent on detector geometry. In Table 5 examples 8, 15, 16, 17 differ considerably in the detector geometry (see Figure 13) yet B/Δ varies only from 3.90 to 4.16.

4. Table 5 also lists [GF], and [GF]/B. Examples 1 through 14 which have identical detector geometry differ in the value of θ_p. The peak value of GF(E) changes slightly as is shown in Figure 15 in which GF(E) is plotted for two extreme cases. The values of [GF]/B in Table 5 show that

$$[GF] \propto B \qquad 8.2$$

for these examples. [GF] in the table is given for unit energy. At other energies the numerical value is T_p times [GF]. If T_p is in keV the units of [GF] are then cm^2sterkeV.

5. [GF] is approximately proportional to the area of the detector. This is demonstrated by examples 8, 15, 16 in Table 5 which have identical detectors, mounted in different radial positions (Figure 13). [GF] and B are very nearly the same in all three cases. Hence a given area contributes the same to [GF] whatever its radial position. There is a small change in the energy at which the peak value occurs. These examples also show that misalignment of the detector in the construction of a unit has only a small effect on its performance, as long as it remains entirely between the plates in its radial position.

6. The angular response parallel to the cylindrical axis may be approximated by Y/ℓ if it is small, and from 7.1 it is clear that $[GF] \propto \Delta^2$. The results of this section can be combined by writing

$$\frac{[GF]}{T_p} = K\ \Delta\ B\ A\ Y/\ell \qquad 8.3$$

where A is the detector area, B is given by 8.1 and K is a proportionality factor whose value and constancy remain to be determined. Its value is listed in Table 5. It ranges from 2.27 to 2.77 with most values lying between 2.50 and 2.70. Using a value of 2.6 for K in Equations 8.1 and 8.3, B and [GF] can be estimated to within about 10% which is adequate in the design stage of an experiment.

7. The results can be adapted for analyzers with non-symmetric plate voltages. If the potential of the mid-plane is V_m, in the fringe field the particles are first all accelerated by V_m and then enter an analyzer with symmetric voltages. Using Equation 2.5

$$GF'(E) = \left(\frac{E - eV_m}{E}\right)^{\frac{1}{2}} GF(E - eV_m)$$

where GF'(E) is the required geometric factor.

8. Both Reidler[17] and Theodoridis and Paolini[16] give numerical examples of the results of their calculations. In each case the detector covers the complete gap between the plates. The numerical specifications of their analyzers has been read into the computer program used to obtain the results above thus allowing a comparison between the three methods. The voltage between the plates is such as to give T_p = 1 keV in all the examples.

Reidler[17] calculates [GF] for analyzers with $\theta_p = 64^o$ and 127^o but otherwise identical. He finds at $\theta_p = 64^o$ [GF] = 3.07×10^{-3} cm^2 sterkeV and at $\theta_p = 127^o$ [GF] = 2.04×10^{-4} cm^2sterkeV. Using our method with his dimensions gives

$$\text{at } \theta_p = 64^o \quad [GF] = 1.06 \times 10^{-3} \text{ cm}^2\text{sterkeV}$$

$$\text{and at } \theta_p = 127^o \quad [GF] = 1.87 \times 10^{-4} \text{ cm}^2\text{sterkeV}.$$

At 127^o there is reasonable agreement but the difference at 64^o is considerable. However, Reidler states that the results at 64^o are doubtful because some of the assumptions made are less accurate for smaller angles.

Theodoridis and Paolini only give a calculation for $\theta_p = 180^o$ but by using a curve published by them elsewhere[20] it may be adapted to 127^o. For their analyzer, with dimensions somewhat greater than Reidler's, they get

$$[GF] = 1.9 \times 10^{-2} \text{ cm}^2\text{sterkeV}$$

Using our method gives

$$[GF] = 3.23 \times 10^{-2} \text{ cm}^2\text{sterkeV}$$

Reidler's results may also be applied to this analyzer giving

$$[GF] = 3.36 \times 10^{-2} \text{ cm}^2\text{sterkeV}$$

Theodoridis and Paolini's result differs significantly from the other two. They also comment on the high energy tail in the response of the cylindrical analyzer in comparison with the spherical analyzer. However, this is not a property of the cylindrical analyzer but rather the abnormally large angular response parallel to the cylindrical axis of their analyzer. With a narrower angular response the response curve is more nearly symmetric, as is shown in Figure 15.

9. FRINGE FIELD EFFECTS

Throughout the analysis the electric field has been taken to be the ideal, radial field, inversely proportional to r and limited to the region between the plates. The fact that the real field is different modifies the trajectories and therefore also affects the geometric factor. The real field differs from the ideal field near the ends of the analyzer plates. In order to simplify estimates of the effect of the fringing field at the entrance it can be separated into three different parts. Although this is neither real nor adequate for a proper calculation of the particle trajectory in the fringe field it suffices for a calculation of the order of magnitude of the deviation from the ideal.

At the entrance to the plates there is a tangential field which either accelerates or decelerates the particles. If the particle does not enter the plates at the radial position where the potential is zero it's kinetic energy is changed. This effect is allowed for in the analysis simply by taking account of the difference in potential.

The radial field just inside the plates is weaker than the ideal. Morse and Feshbach[19] give a solution for the electric field near the edge of a semi-infinite parallel plate capacitor which may be used to estimate the field near the end of the analyzer plates. The radial field along the midplane is plotted in Figure 16. It reaches 95% of the ideal value .3d from the end (d is the distance between the plates). The magnitude of the effect on a particle trajectory can be calculated by considering the field to exert an impulse on a particle as it traverses this short distance .3d between the plates.

$$\text{Impulse } I = \int eE_{\perp} dt = \frac{e}{\dot{x}} \int_0^{.3d} E_{\perp}\, dx \qquad 9.1$$

The particle is assumed to be moving along the midplane as if in a circular orbit. Ideally it is deflected through an angle $\delta\theta = I/m\dot{x} = .3d/r$ Integrating the curve in Figure 16 as in Equation 9.1 shows that the actual impulse is only .88 times the ideal impulse i.e., the trajectory is deflected only .88 $\delta\theta$. The deviation from ideal is .12 $\delta\theta$ which gives a maximum radial displacement of .02Δ times the plate spacing. This displacement affects the geometric factor by changing the limiting trajectories which graze the plates at the entrance. The effect is so slight that it may be ignored.

Outside the plates there is a radial electric field where ideally there is none. The total impulse as the particle enters the analyzer is greater than the ideal impulse. There is a net deflection of the trajectories towards the inner plate. This has no effect on the geometric factor unless there is some structure near the entrance which intercepts the trajectories. For these theoretical calculations to be accurate the entrance aperture (as in Figure 1) must be wider than the plate spacing to allow for the deflection in the fringing field.

The trajectories are not all deflected by the same amount. The effect of the relative deflections is allowed for by the factor N in Equation 2.5. No other published calculations of geometric factors have allowed for the net or relative deflections in the fringe field. At the exit from the analyzer near the detector surface the electric field also differs from the ideal. In this region few limiting trajectories are affected but the

position at which particle strikes the detector may be changed. Deviations are of the same order of magnitude as at the entrance and are thus much smaller than inaccuracies of the approximations.

In conclusion, as long as the entrance aperture does not obstruct particles which would otherwise pass between the plates the fringe field has only a small effect on the geometric factor.

ACKNOWLEDGMENTS

Part of this work was carried out while the author held a NAS/NRC Resident Research Associateship at NASA-Goddard Space Flight Center.

REFERENCES

1. Evans, D. S., Rev. Sci. Inst. 36, 375 (1965).
2. Bame, S. J., J. R. Asbridge, H. E. Felthauser, R. A. Olsen, and I. B. Strong, Phys. Rev. Letters, 16, 138 (1966).
3. Chase, L. M., J. Geophys. Res. 75, 7128 (1970)
4. Wolfe, J. H., R. W. Silva, and M. A. Myers, J. Geophys. Res., 71, 1319 (1966).
5. Bryant, D. A., G. M. Courtier, and A. D. Johnstone, Journ. Atmos. Terres. Phys., 31, 579 (1969).
6. DeForest, S. E., and C. E. McIlwain, J. Geophys. Res., 76, 3587 (1971).
7. Frank, L. A., J. Geophys. Res., 72, 185 (1967).
8. Hoffman, R. A. and D. S. Evans, J. Geophys. Res. 73, 6201, (1968).
9. Lind, D., and N. McIlwraith, IEEE Trans. Nucl. Sci., 13, (1966).
10. O'Brien, B. J., F. Abney, J. Burch, R. Harrison, R. LaQuey, and T. Winiecki, Rev. Sci. Inst., 38, 1058 (1967).
11. Heikkila, W., J. B. Smith, J. Tarstrup, and J. D. Winningham, Rev. Sci. Inst. 41, 1393 (1970).
12. Chase, L. M., J. Geophys. Res., 73, 3469 (1968).
13. Hughes, A. L., and V. Rojansky, Phys. Rev., 34, 284 (1929).
14. Dempster, A. J., Phys. Rev., 51, 67 (1937).
15. Herzog, R., Zeit. fur. Phys., 89, 447 (1934).
16. Theodoridis, G. C., and F. R. Paolini, Rev. Sci. Inst., 39, 326 (1968).
17. Reidler, W., Kiruna Geophysical Observatory preprint number 70-311 (1970).
18. Goldstein, H., Classical Mechanics, p. 64, Addison-Wesley (1950).
19. Morse, P. M., and H. Feshbach, Methods of theoretical physics, p. 1245, McGraw Hill (1953).
20. Paolini, F. R. and A. C. Theodoridis, Rev. Sci. Inst., 38, 579 (1967).

TABLE CAPTIONS

1. Numerical solutions for the radial turning points (equation 3.3) when H=1.
2. The expressions to be used in calculating the geometric factor in regions A, B and C of Figure 9.
3. A comparison between N sin α calculated by the exact expression and tan α calculated for the approximate trajectory. For this trajectory H=1, T=0.98.
4. The integrated geometric factor [GF] of 127^{o} analyzers calculated exactly and using the approximate trajectory equation.
5. The results of calculations of the geometric factor and energy bandwidth of various practical analyzers.

TABLE 1

T	ρ_{10}	ρ_{20}	ρ_{10}^{-1}	$1-\rho_{20}$
0.96	1.138	0.855	.138	.145
0.97	1.120	0.875	.120	.125
0.98	1.098	0.898	.098	.102
0.99	1.070	0.928	.070	.072
1.00	1.0	1.0	0	0

TABLE 2

Region	$N\sin\alpha_1$	$N\sin\alpha_2$
A	4.10a	4.11b
B	4.10a	4.11a
C	4.10b	4.11a

TABLE 3

ρ	$N\sin\alpha$	$\tan\alpha$
.9	.036	0
.92	.090	.085
.94	.116	.113
.96	.132	.130
.98	.141	.139
1.00	.143	.141
1.02	.141	.139
1.04	.132	.130
1.06	.115	.113
1.08	.087	.085
1.10	0	0

TABLE 4

r_i	r_o (cms)	$[GF_\perp]$ (cm-radian x 10^4) exact	approximate
.975	1.025	1.5768	1.5768
.950	1.050	12.631	12.633
.925	1.075	42.829	42.868
.900	1.100	102.07	102.24

TABLE 5

	θ_p degrees	Δ	B	B/Δ	[GF] cm^2 ster x 10^4	[GF]/B x 10^4	AY/ cm^2 radian x 10^3	K	Detector Geometry Fig. 13
1	125	.05	.101	2.02	.482	4.77	3.70	2.76	c
2	120	.05	.110	2.20	.524	4.76	3.70	2.70	c
3	115	.05	.121	2.42	.569	4.71	3.70	2.64	c
4	110	.05	.130	2.60	.623	4.80	3.70	2.61	c
5	105	.05	.144	2.88	.687	4.76	3.70	2.56	c
6	100	.05	.160	3.20	.765	4.78	3.70	2.53	c
7	95	.05	.178	3.57	.860	4.82	3.70	2.51	c
8	90	.05	.204	4.08	.978	4.79	3.70	2.50	c
9	85	.05	.235	4.70	1.125	4.79	3.70	2.51	c
10	80	.05	.274	5.49	1.311	4.79	3.70	2.53	c
11	75	.05	.323	6.46	1.511	4.69	3.70	2.49	c
12	70	.05	.390	7.80	1.867	4.79	3.70	2.61	c
13	65	.05	.477	9.54	2.294	4.81	3.70	2.67	c
14	60	.05	.592	11.8	2.892	4.81	3.70	2.68	c
15	90	.05	.195	3.90	.884		3.70	2.27	e
16	90	.05	.206	4.12	1.024		3.70	2.63	d
17	90	.1	.416	4.16	36.10		32.9	2.61	f
18	60	.025	.280	11.2	1.525		7.86	2.76	b
19	70	.0254	.192	7.56	.122		.928	2.64	a

FIGURE CAPTIONS

Figure 1. The basic geometrical definitions of the analyzer and detector combination.

Figure 2. The motion of a group of particles through a two-dimensional analyzer shown in a general way. The region of phase space occupied by the particles is shown shaded in the pair of diagrams at each point P, Q.

Figure 3. The quantity ν defined in the text is a measure of the accuracy of the approximation $\rho_{10} - 1 = 1 - \rho_{20}$. For most orbits in practical analyzers $T > 0.96$.

Figure 4. In this diagram and subsequent diagrams through Figure 8, the analyzer plates are shown as parallel straight lines with the distance between exaggerated greatly. The trajectories can then be shown as sinusoidal curves. The detector is shown at the radial position ρ.

Figure 5. The limiting trajectories in an analyzer with $\theta_p = \pi/\sqrt{2}$.

Figure 6. The limiting trajectories in an analyzer with θ_p between $2^{-3/2}\pi$ and $2^{-1/2}\pi$. One trajectory grazes a plate at the entrance aperture and the other grazes a plate at its radial turning point.

Figure 7. This diagram shows the limiting trajectory which grazes a plate at the entrance and at its radial turning point.

Figure 8. The limiting trajectory when $M > \rho_o$ and $N \sin \alpha_1$ is negative.

Figure 9. This diagram illustrates the region A, B, C in x-m space where the various expressions for N sin α must be used. The correct expressions are listed in Table 2. The bounding curves are (i) given by equation 4.13b, (ii) by 4.12b, (iii) by 4.12a, and (iv) by 4.13a. The coordinate m is a function of energy so that the extent parallel to the m-axis is an indication of energy bandwidth. The coordinate x indicates the radial position of a detector element. The lines $x = \pm 1.0$ are the analyzer plates.

Figure 10. The angle between the trajectory and a tangent to the cylindrical surface for both the real trajectory and the approximate trajectory as a function of radial position.

Figure 11. The quantity ϵ (defined in the text as a measure of the difference between exact and approximate values of GF(H)) as a function of H. The limits marked on the diagram are the energy limits for analyzers with the indicated values of Δ.

Figure 12. A particle trajectory projected on to the cylindrical surface shown flattened in the diagram.

Figure 13. The shapes and positions of detectors relative to the analyzer plates for the examples listed in Table 5. The detector's sensitive surface is shown shaded.

Figure 14. Energy bandwidth as a function of the sector angle θ_p of the analyzer.

Figure 15. The energy-dependent geometric factor for two extreme values of θ_p.

Figure 16. The fringe field at the edge of a semi-infinite parallel plate capacitor. E is the radial field at the midplane between the plates. E_o is its ideal value.

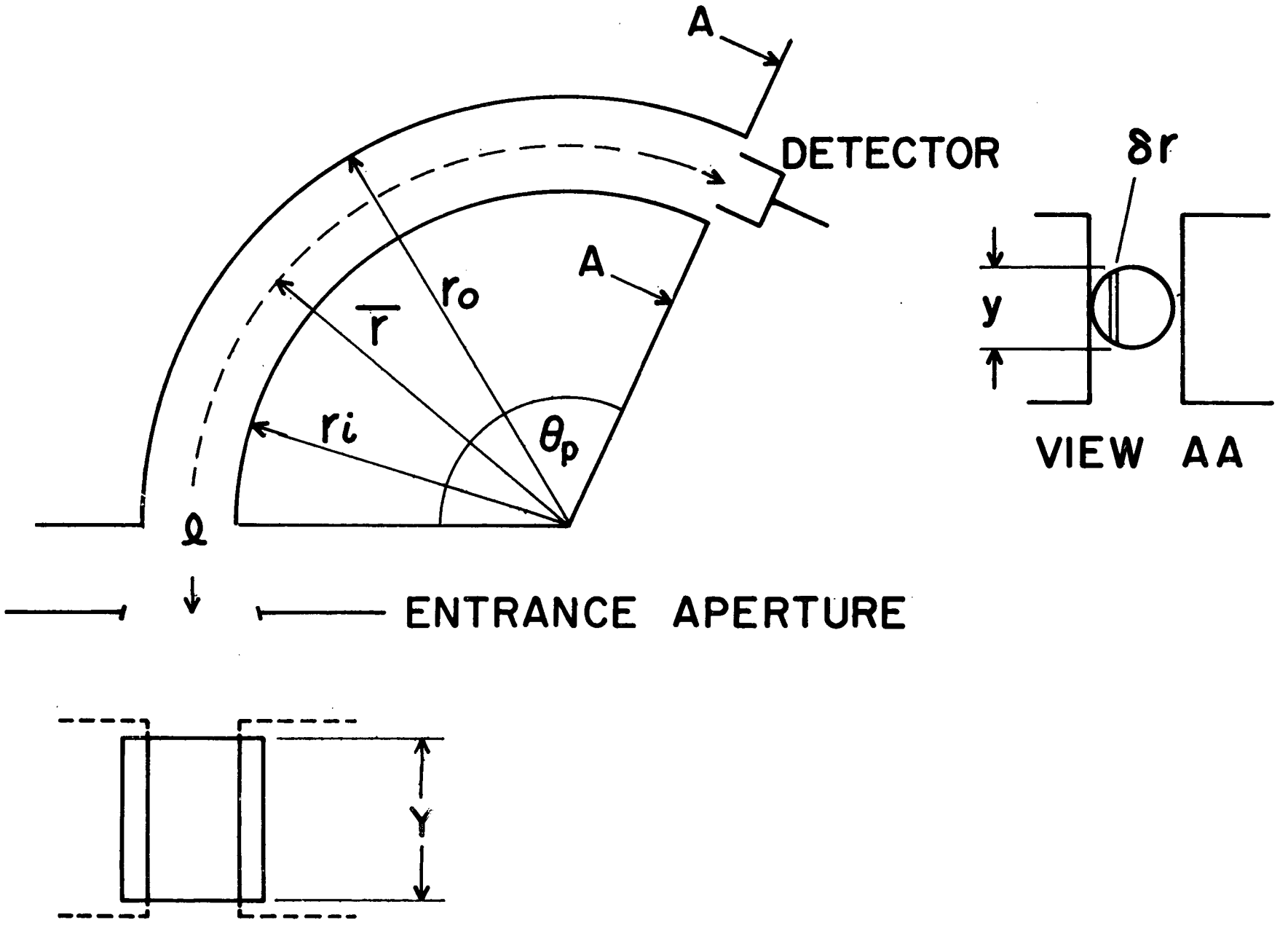
A
DETECTOR
δr
A
r_o
$\bar{r}$
r_i
θ_p
y
VIEW AA
ENTRANCE APERTURE
Y

FIGURE 1

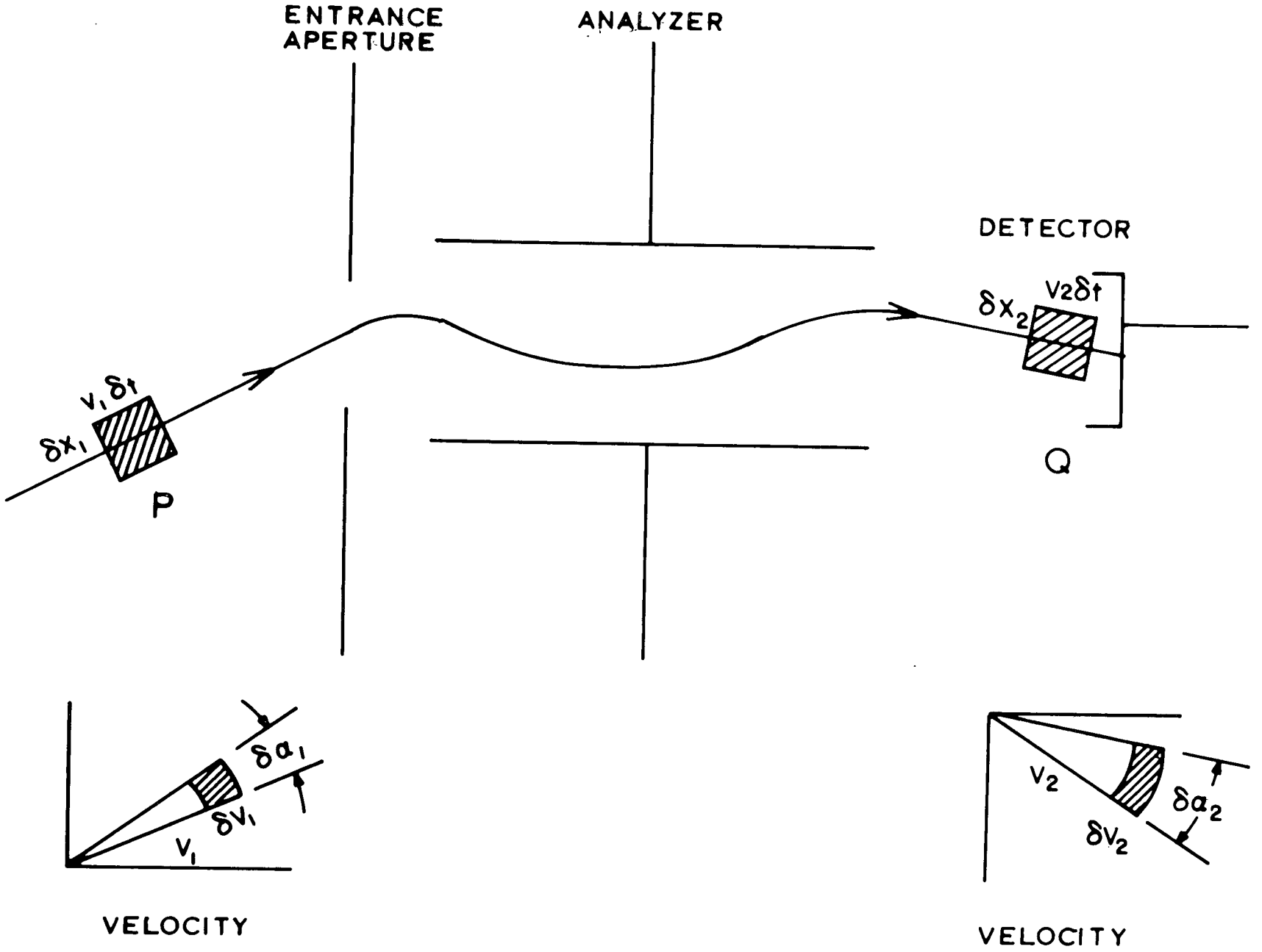
ENTRANCE APERTURE
ANALYZER
DETECTOR
$v_2\delta t$
δx_2
$v_1\delta t$
δx_1
P
Q
δa_1
δv_1
v_1
VELOCITY
v_2
δa_2
δv_2
VELOCITY

FIGURE 2

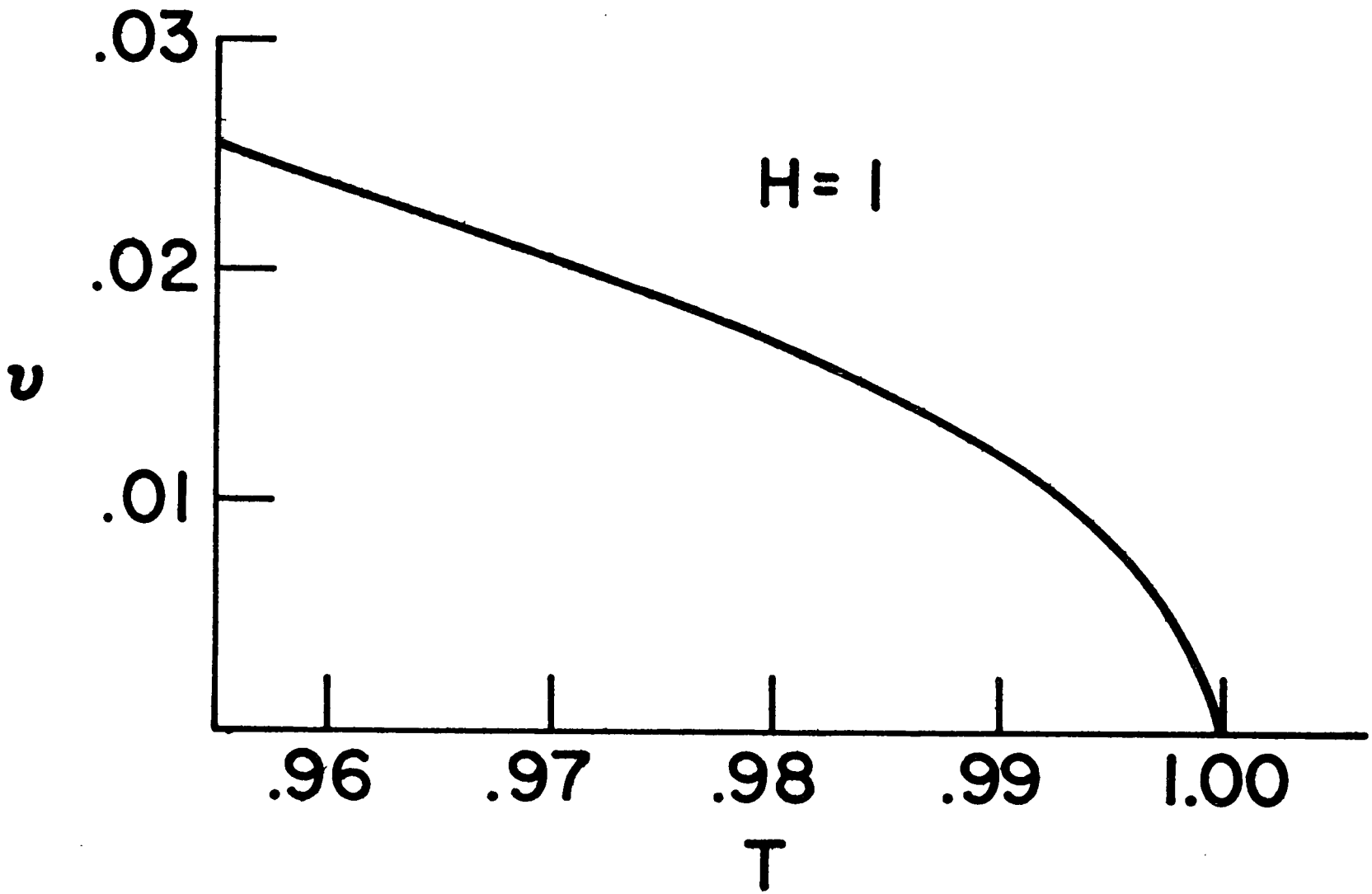

FIGURE 3

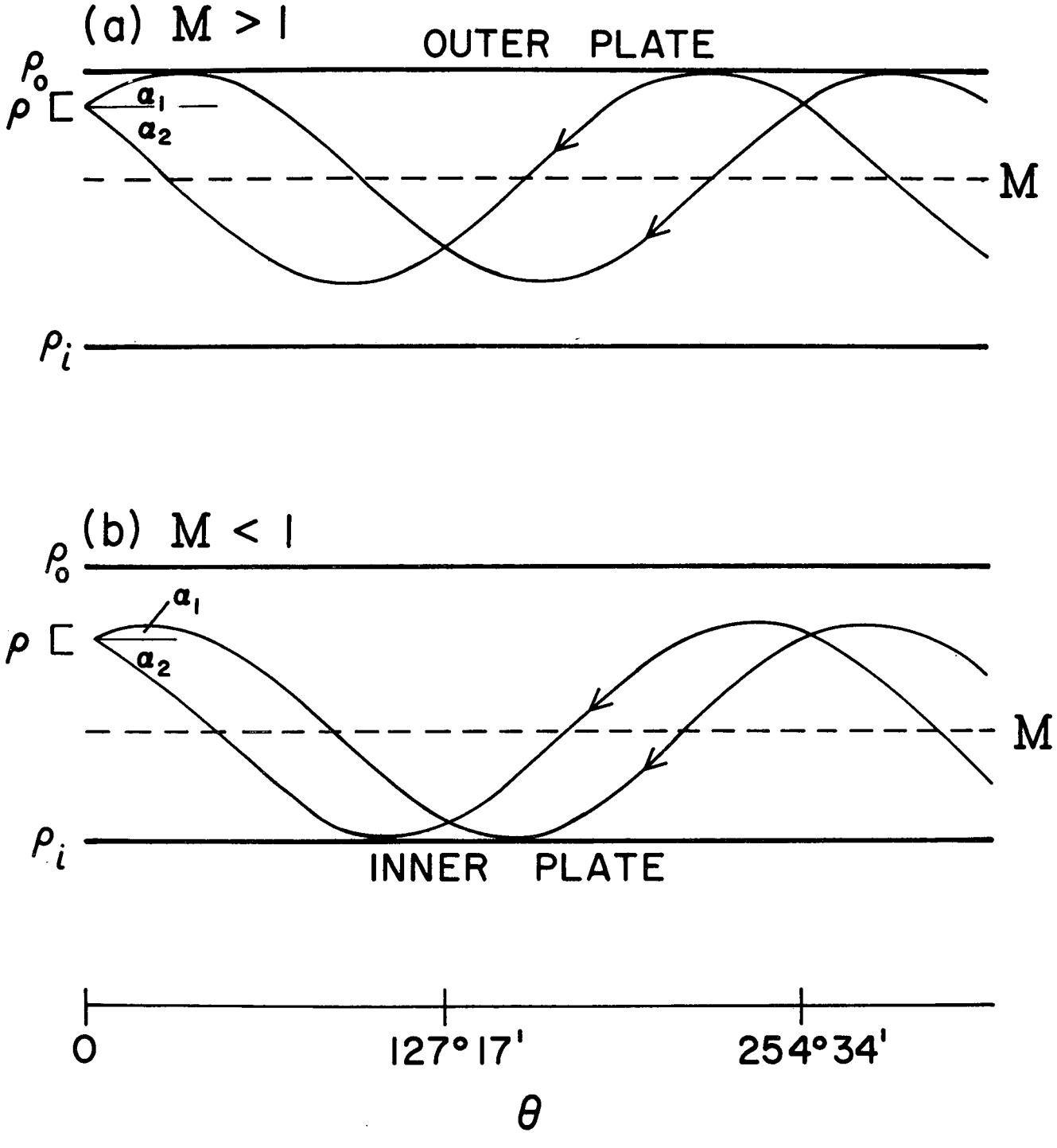
(a) M > 1
OUTER PLATE
ρ_o
ρ
α_1
α_2
M
ρ_i
(b) M < 1
ρ_o
α_1
ρ
α_2
M
ρ_i
INNER PLATE
0
127°17'
254°34'
θ

FIGURE 4

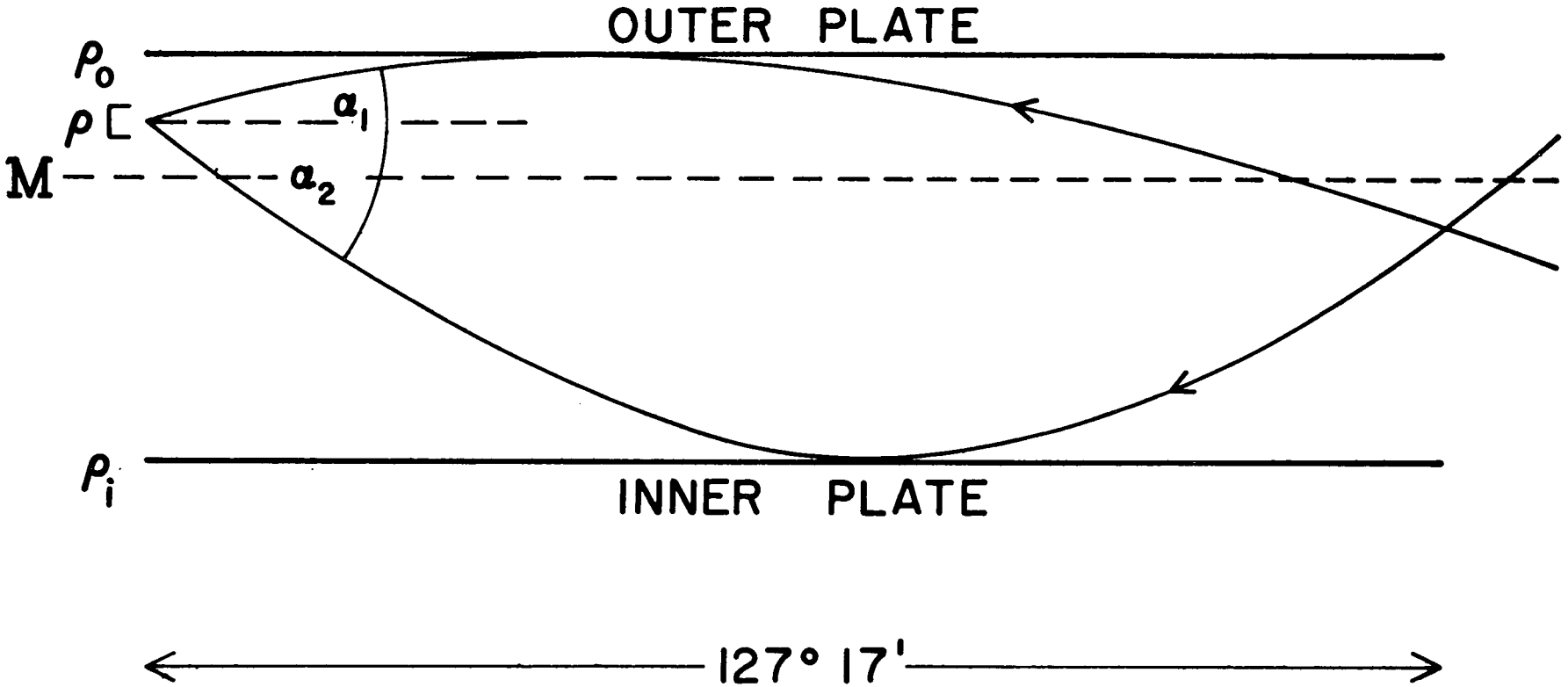

FIGURE 5

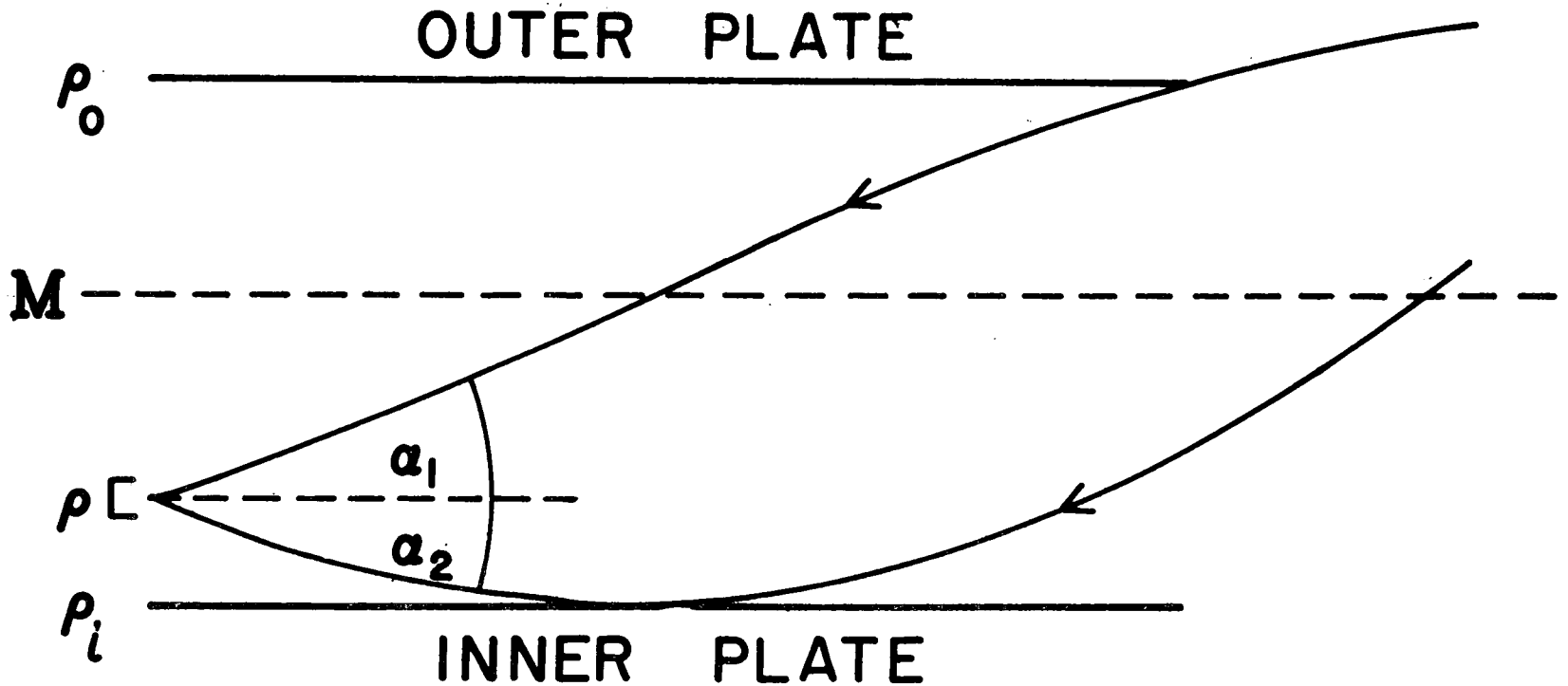

FIGURE 6

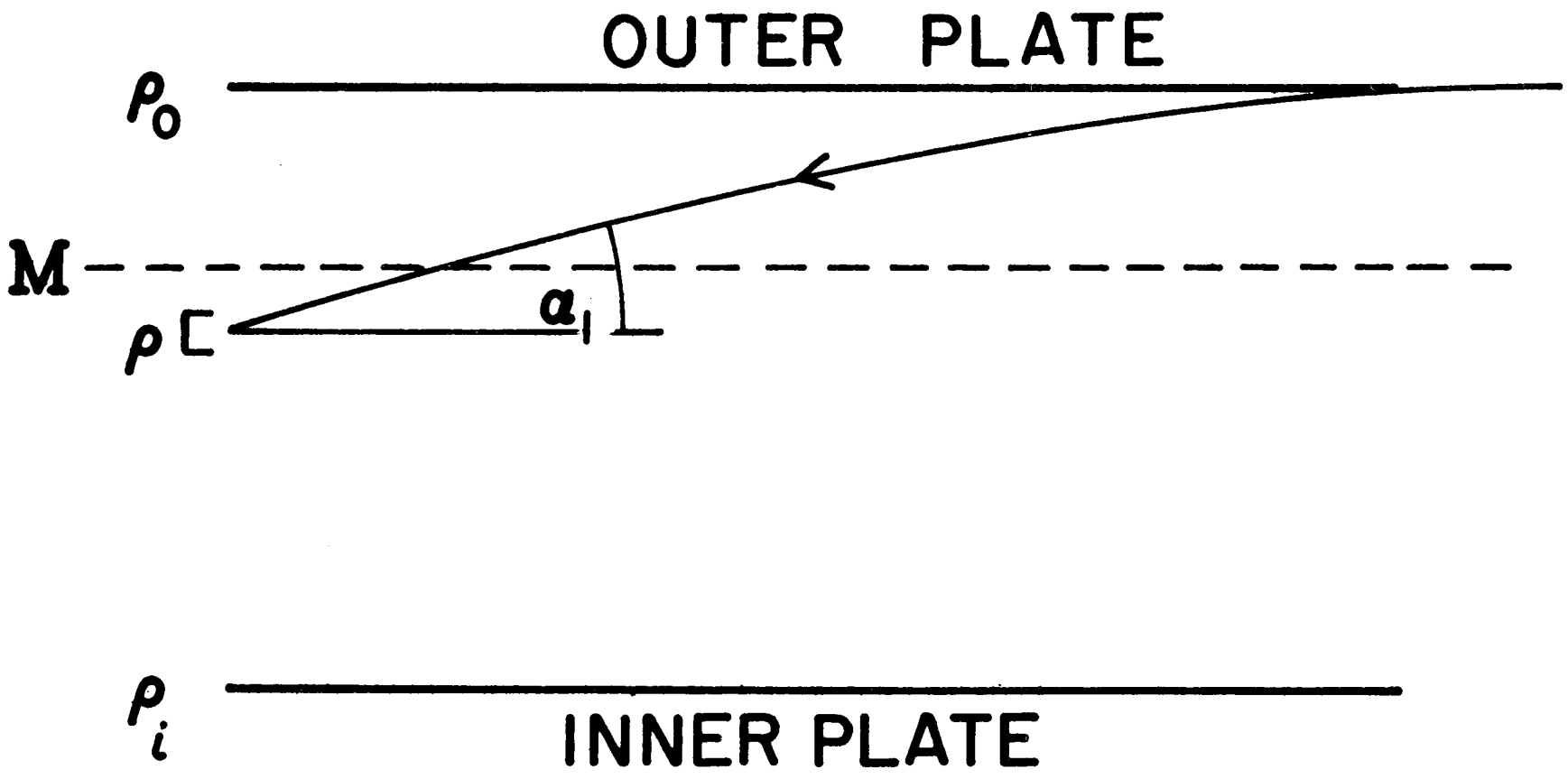

FIGURE 7

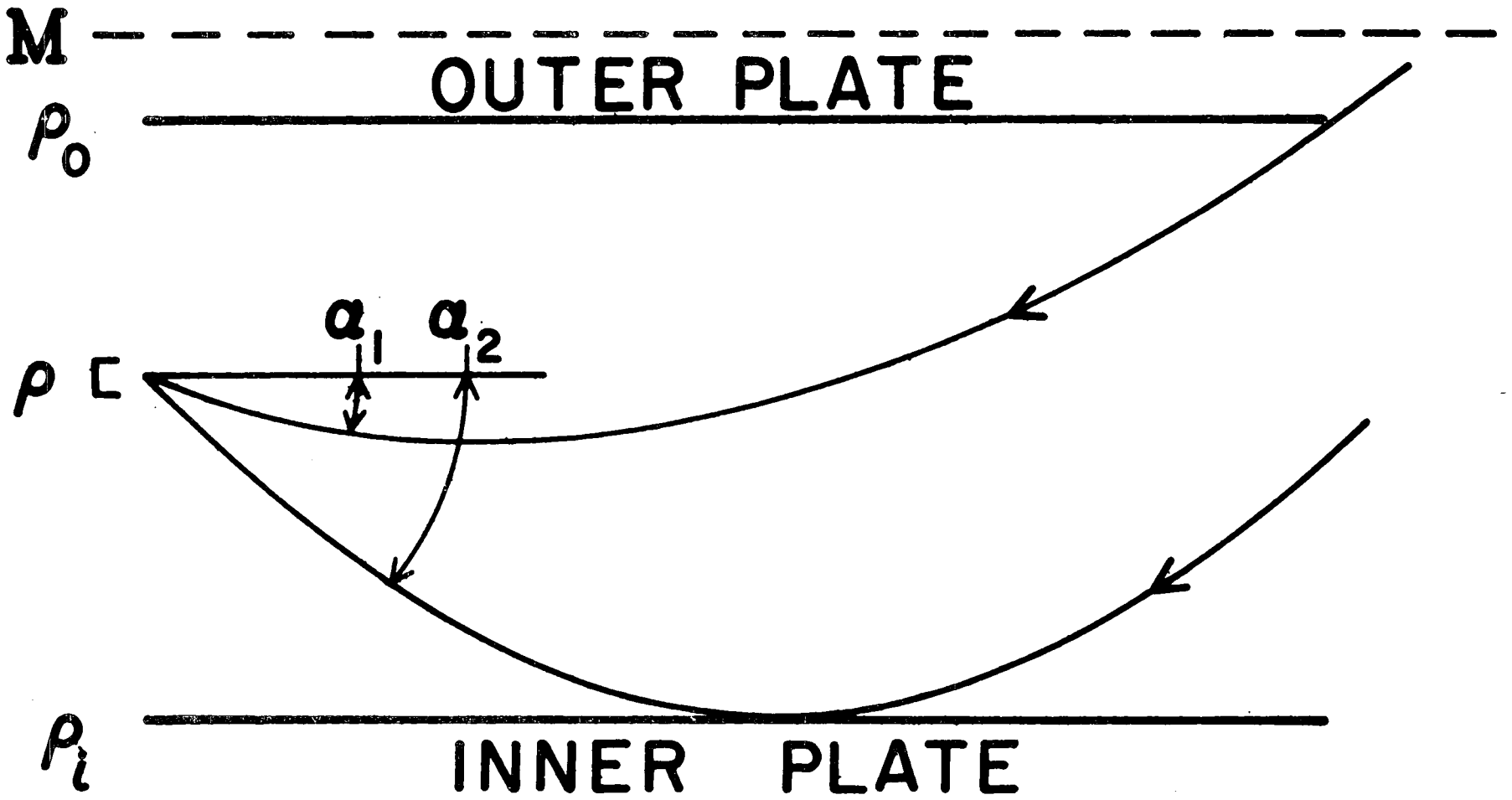

FIGURE 8

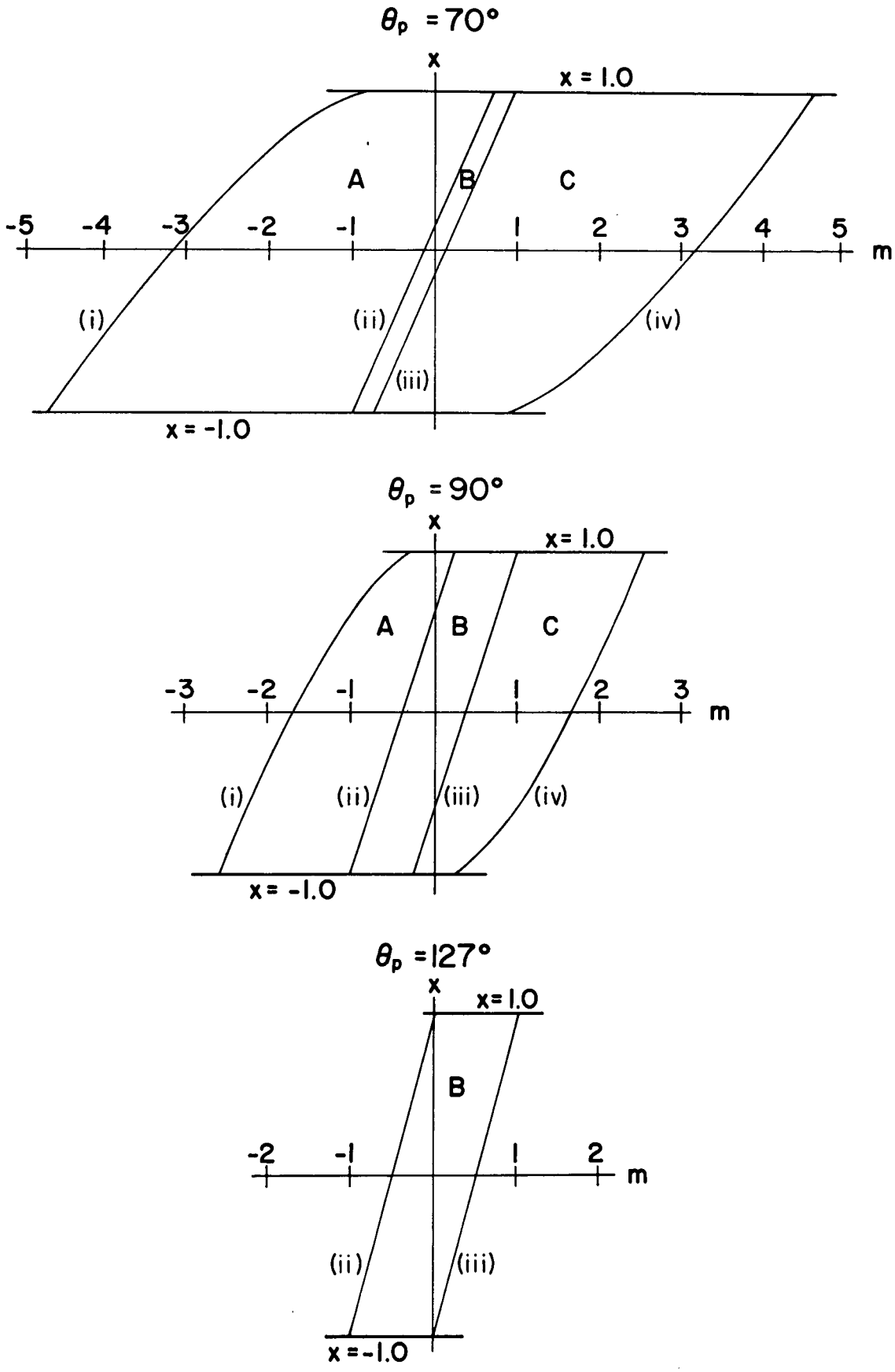
θp = 70°
x
x = 1.0
A
B
C
-5
-4
-3
-2
-1
1
2
3
4
5
m
(i)
(ii)
(iii)
(iv)
x = -1.0
θp = 90°
x
x= 1.0
A
B
C
-3
-2
-1
1
2
3
m
(i)
(ii)
(iii)
(iv)
x= -1.0
θp =127°
x
x=1.0
B
-2
-1
1
2
m
(ii)
(iii)
x =-1.0

FIGURE 9

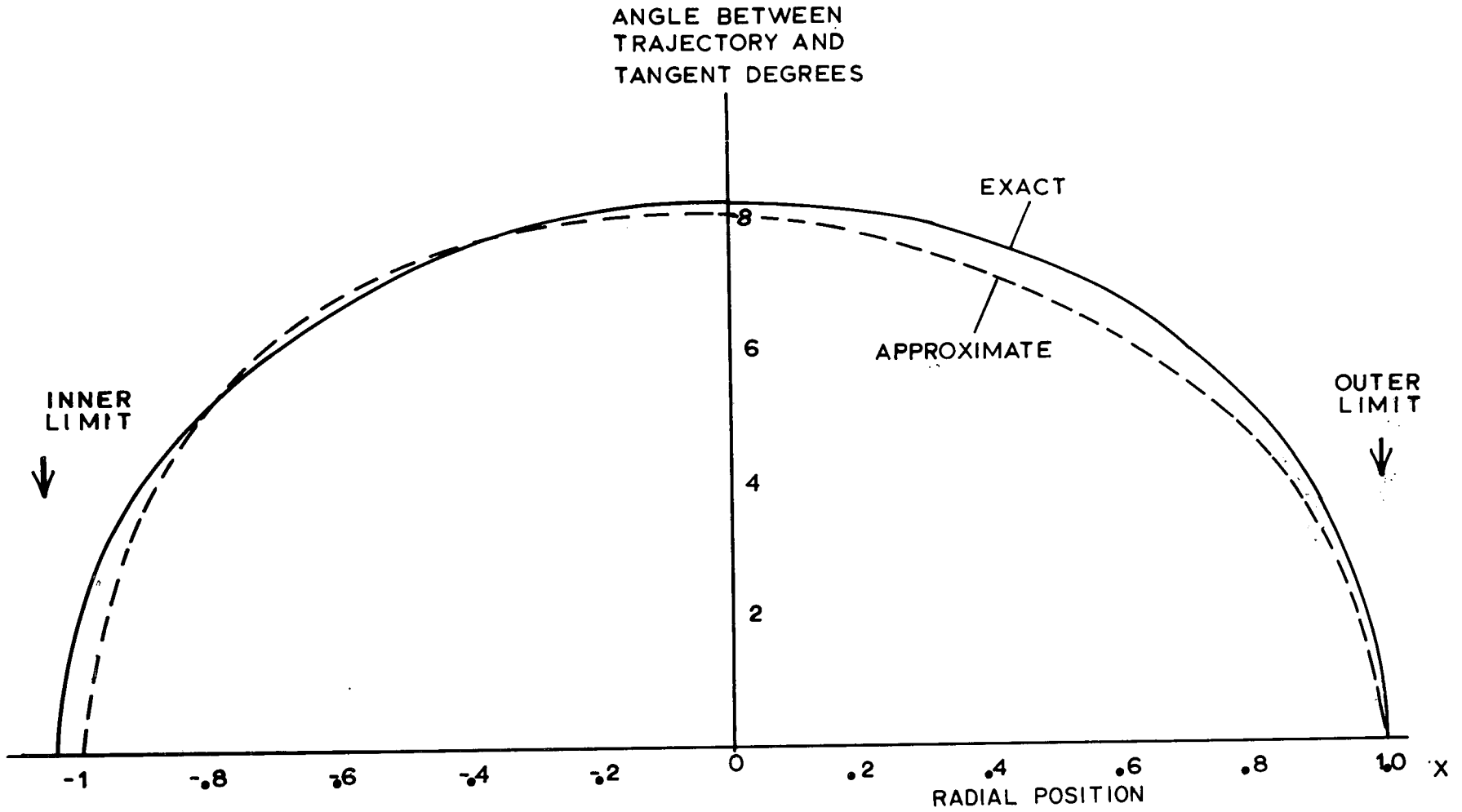
ANGLE BETWEEN
TRAJECTORY AND
TANGENT DEGREES
EXACT
APPROXIMATE
INNER
LIMIT
OUTER
LIMIT
8
6
4
2
-1
-.8
-.6
-.4
-.2
0
.2
.4
.6
.8
1.0
X
RADIAL POSITION

FIGURE 10

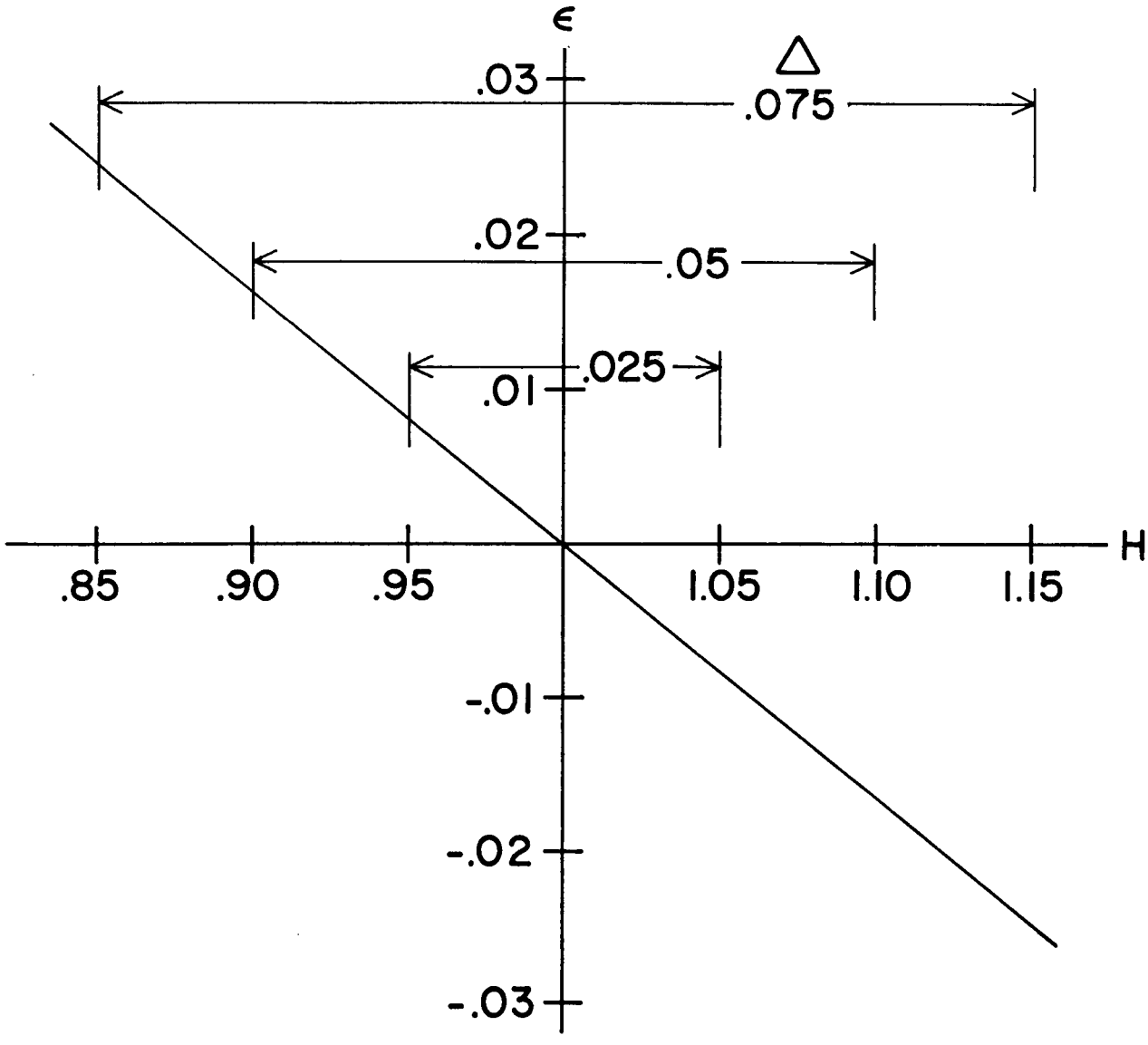

FIGURE 11

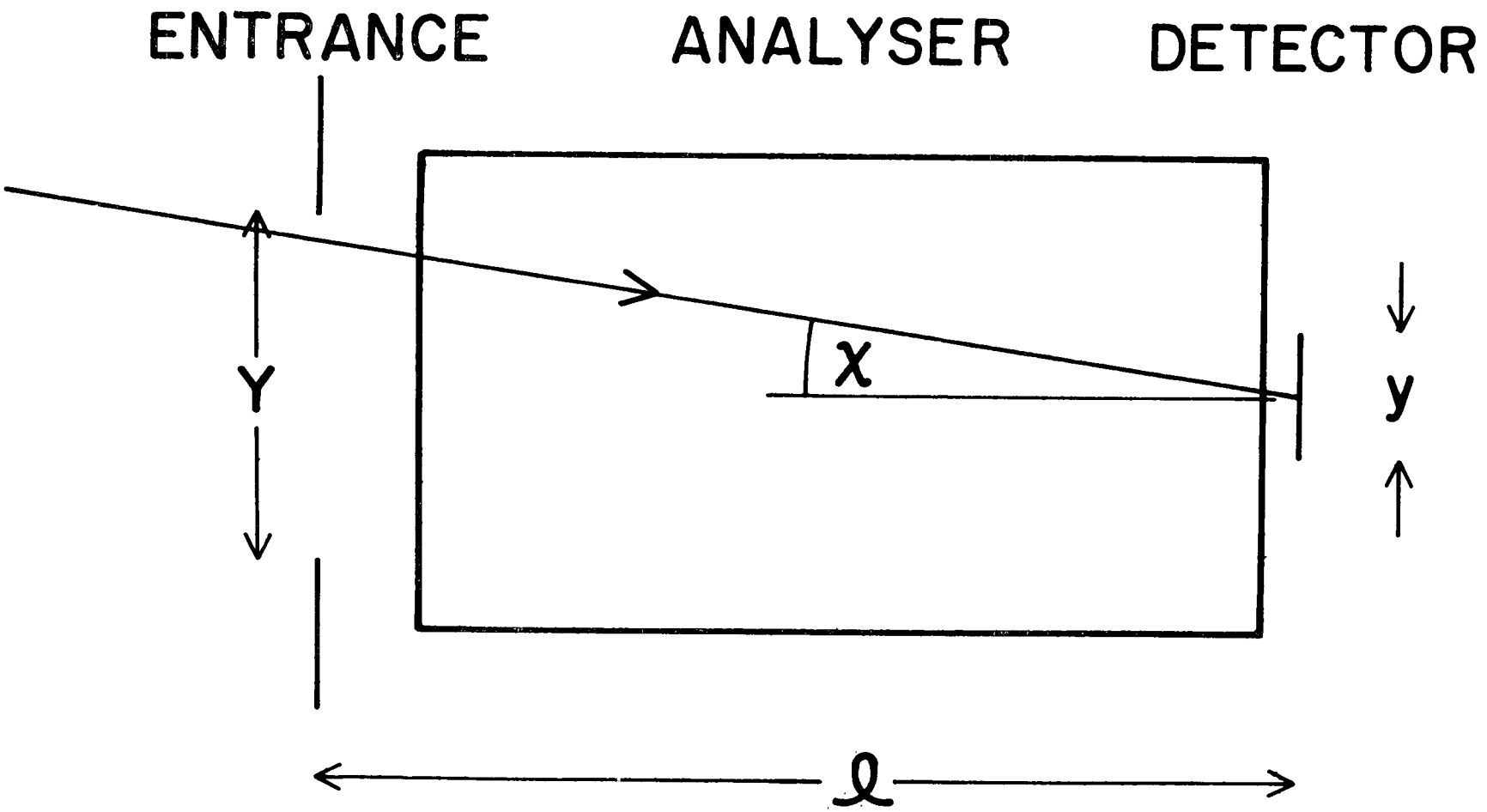

FIGURE 12

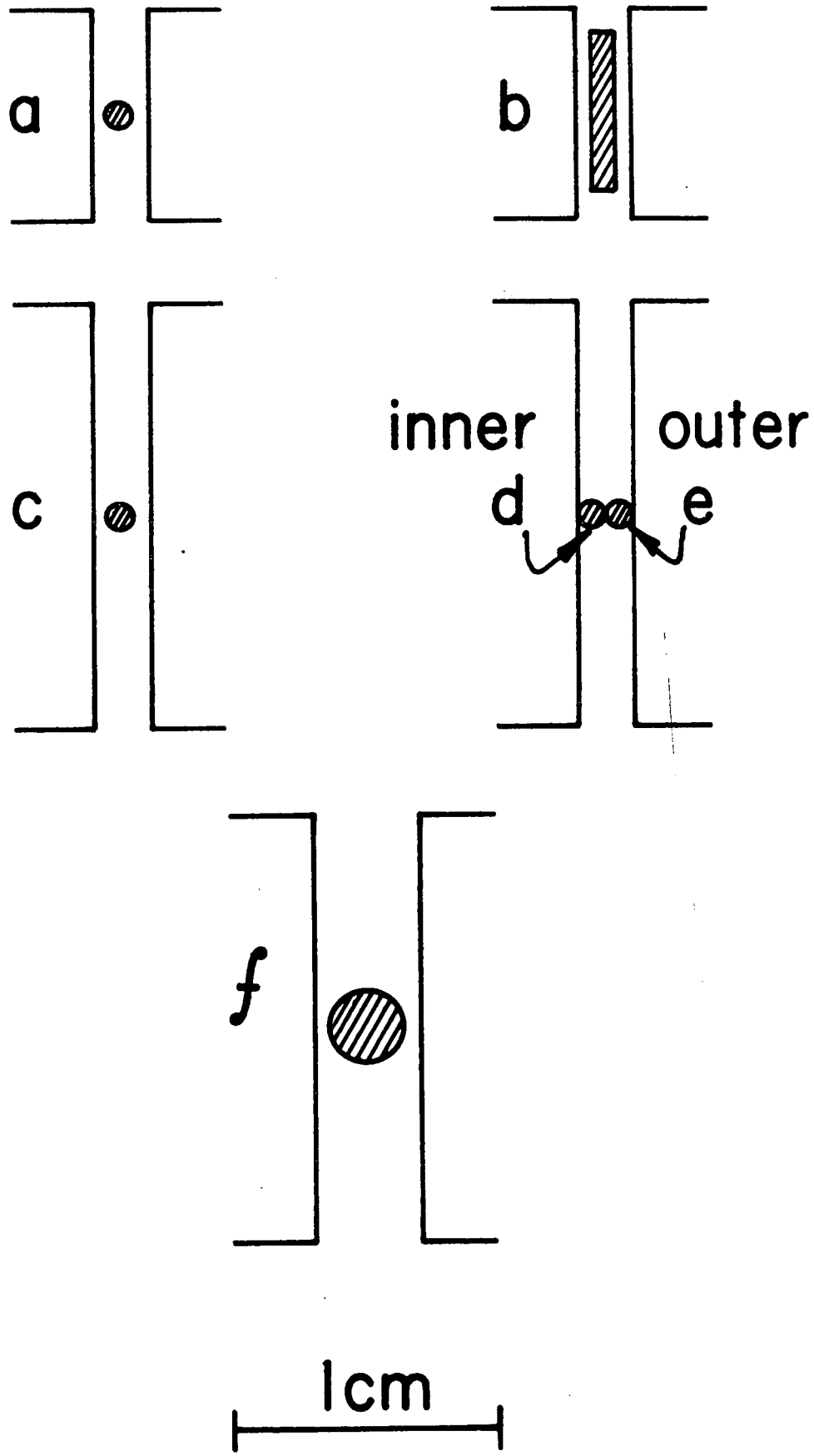

FIGURE 13

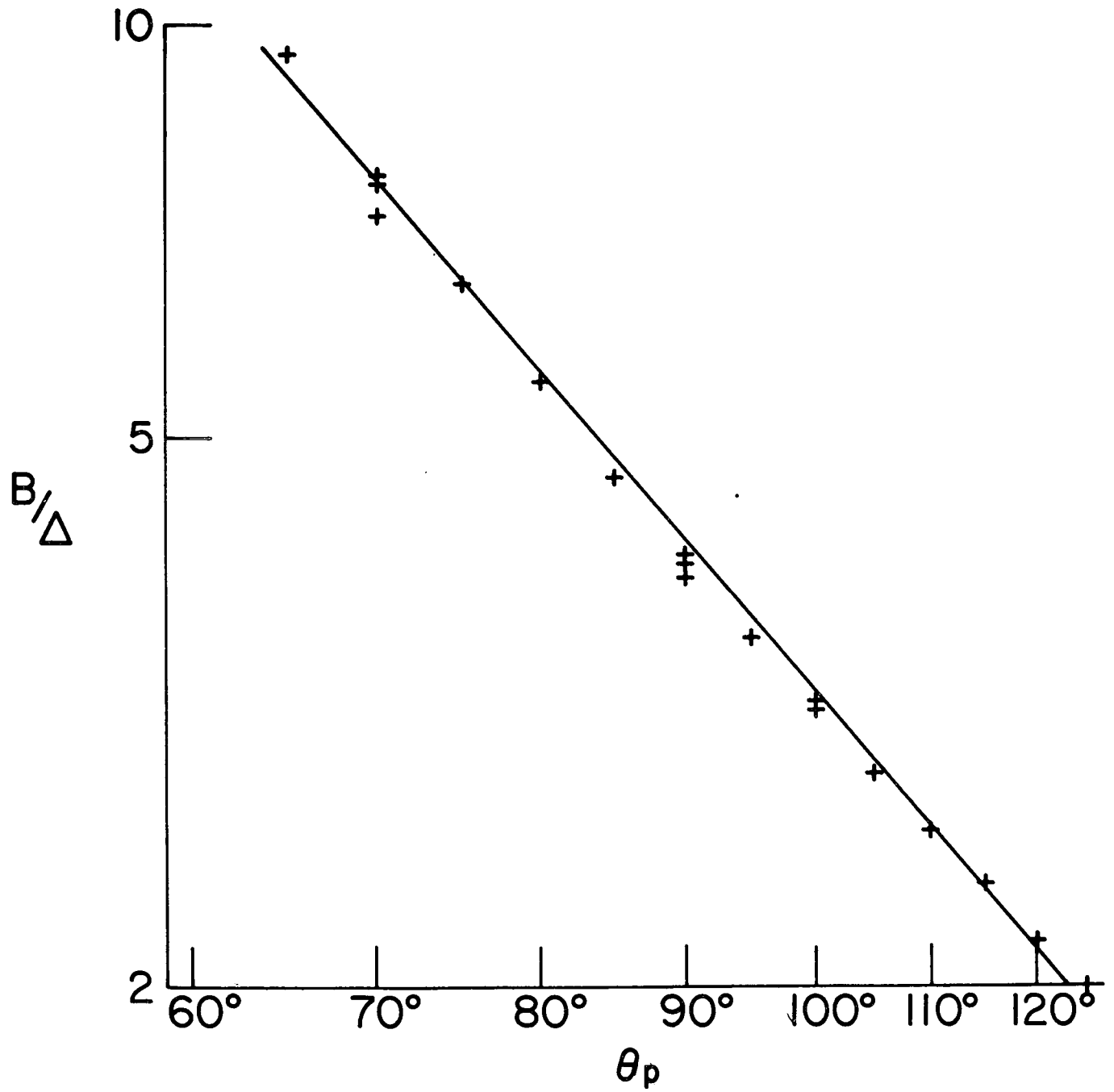

FIGURE 14

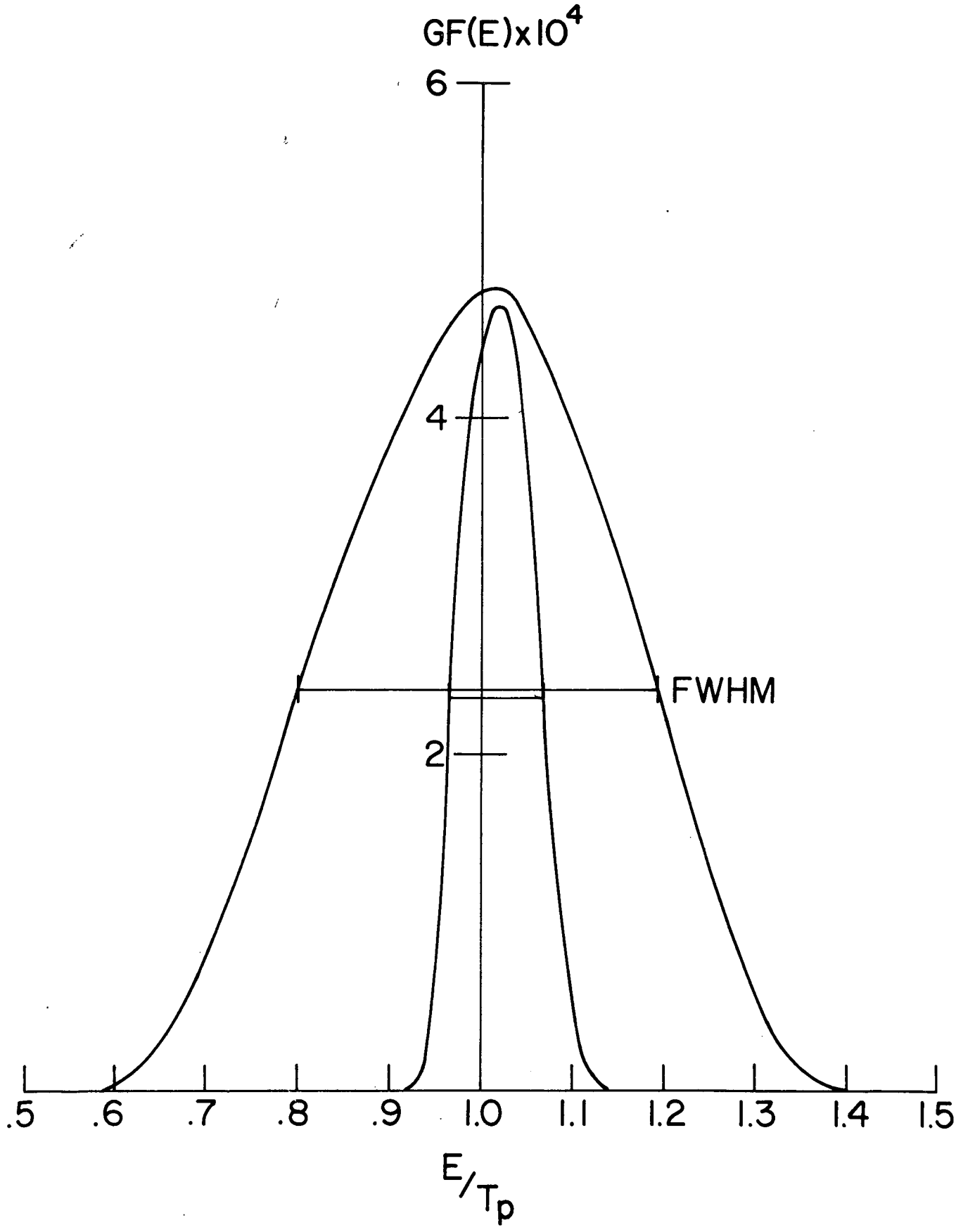

FIGURE 15

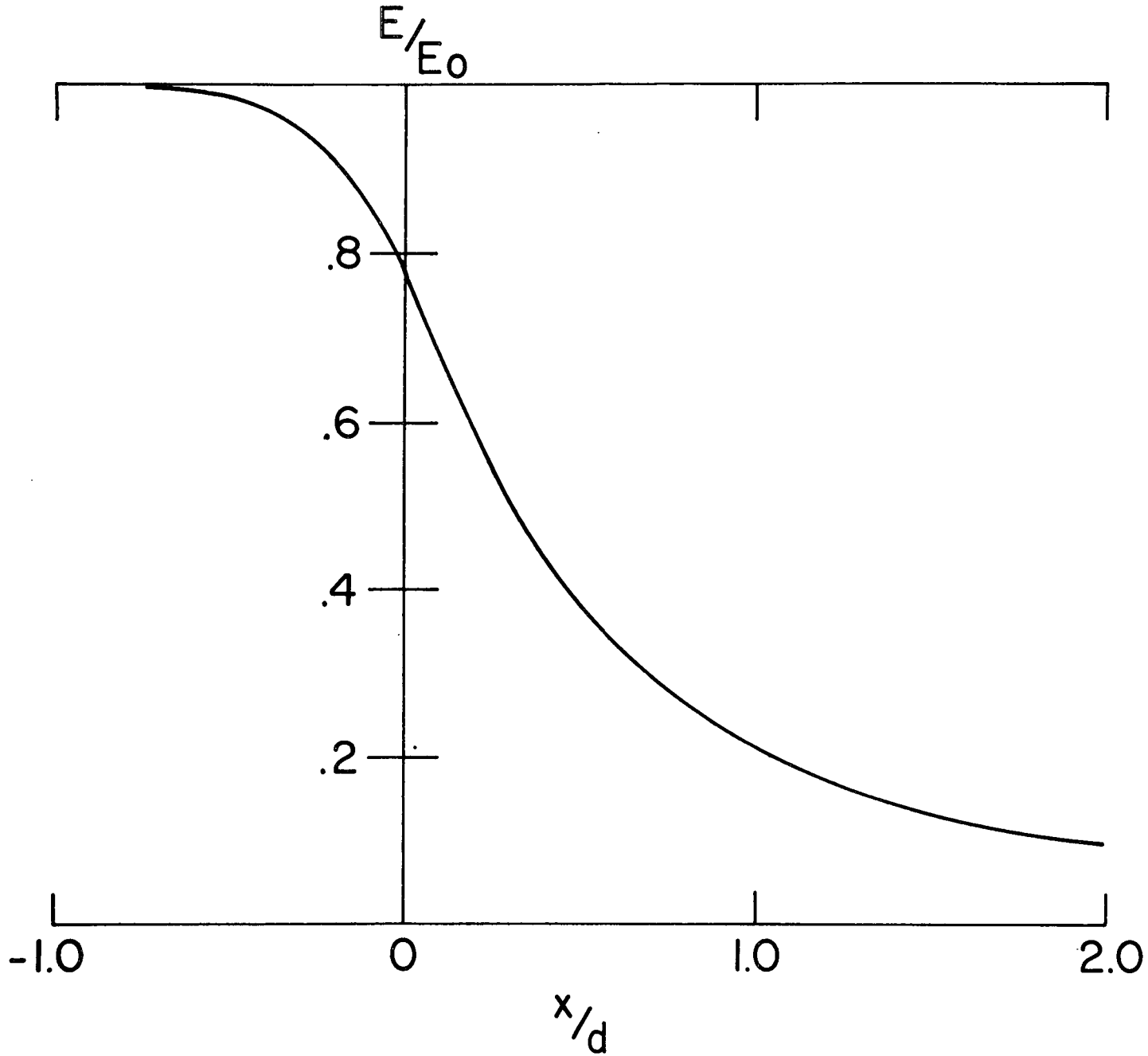

FIGURE 16